NUMERICAL STUDY OF AN INCOMPRESSIBLE LAMINAR FLOW AROUND A NACA AIRFOIL WITH A BLOWING CONTROL.

Submited on 16/01/2018 – Accepted on 03/04/2018

Abstract

A boundary layer separation on a NACA0012 airfoil at a low Reynolds number is numerically investigated. The governing equations are discretized with the finite volume method. The boundary layer separation is examined through the flow structure. Beyond an angle of attack of 8°, a small separation region is detected near the trailing-edge of the airfoil. As the angle of attack increases, the separation region grows up and moves towards the leading edge. In order to control the separation, a parabolic distribution blowing is applied along the separated region. The effectiveness of the control is shown, leading to the improvement of the lift and the lift to drag ratio. As the blowing jet velocity is increased the size of the separation bubble decreases until it disappears.

Keywords: *Boundary layer, Separation control, Aerodynamic performances.*

A BOUNECER
L BAHI

Energy Physics Laboratory, Physics Department, Frères Mentouri University, Algeria.

NOMENCLATURE

C	airfoil chord length
Cd	drag coefficient
Cf	skin friction coefficient
Cl	lift coefficient
Cp	pressure coefficient
h_1	metric parameter in ξ direction
h_2	metric parameter in η direction
P	non-dimensional pressure
Re	Reynolds number
U	horizontal physical velocity
U_0	free-stream velocity
V	vertical physical velocity
Vξ	spanwise computational velocity
Vη	normal computational velocity

Greek symbols

α	angle of attack
ϕ	maximum blowing velocity ratio
τ	non-dimensional time
ρ	density

Subscripts

x	horizontal direction
y	vertical direction
ξ	spanwise direction
η	normal direction to the airfoil

1. INTRODUCTION

The advances in micro-fabrication techniques and miniaturization electronics are leading to the development of small Unmanned Aerial Vehicles (UAVs), Micro-Aerial-Vehicles (MAVs), and small wind turbines. Due to their small length scale of about a few centimeters, the MAV's have the ability to fly in urban settings, tunnels and caves and maintain forward and hovering flight maneuver in constrained environments [1-3]. The small scale of such technological applications combined to their relatively low speed, is the main driving factor for the increasing interest of the low Reynolds number flows over airfoils. Also, this increasing importance is driven by the poor data base of the aerodynamic characteristics of the airfoils operating at low Reynolds numbers (i.e., 10^2-10^5), since most studies on the boundary layer behavior over airfoils have focused on conventional aircraft design with high Reynolds numbers. The boundary layer separation can have a large impact on the performance of any vehicle design.

Laminar separation occurs when a laminar boundary layer is subject to a sufficiently strong adverse pressure gradient. As the pressure increases along the mean flow direction, the flow velocity decreases. If the pressure differential continues, the flow velocity will eventually come to zero and a reversal of the flow will occur [4].

Due to the predominance of viscous effects at low Reynolds number, the flow physics is quite complicated and the boundary layer behaves differently in comparison to its behavior at high Reynolds number. The boundary layer starts to separate at a lower angle of attack as a result of the airfoil curvature changes or the adverse pressure gradient [5]. At a low Reynolds number, the boundary layer often remains laminar in the adverse pressure gradient region and the detached boundary layer may undergo transition to turbulence. The resulting turbulent flow may reattach to the airfoil surface. When the turbulent mixing

momentum is not sufficient, the separated region extends up to the trailing edge [6-7]. The location of the separation point, the size of the separated region and the intensity of the backflow, depend on the flow Reynolds number and the angle of attack of the airfoil. These two parameters determine whether the flow reattaches behind the separated zone or remains separated [8].

At a low Reynolds number, the aerodynamic forces are significantly altered by the boundary layer separation and show a different behavior compared to a high Reynolds number flow [9]. Both drag and lift increase with the angle of attack and at a sufficiently low Reynolds number the stall is absent over a large range of angles of attack [10]. Therefore it is desirable to control the flow through the boundary layer. To delay or eliminate the boundary layer separation in order to reduce the drag and increase the lift, different control concepts can be applied, such as the use of the airfoil shaping to create a favorable pressure field capable to overcome the undesirable adverse pressure gradients. Another control mode can be performed with the addition of an energy momentum to the separated boundary layer, to recover the lost energy. Air suction and blowing, vortex generators, surface cooling and moving walls are some examples of the boundary layer separation control [11]. In the experimental investigations, the control process of the separation over small scale airfoils at low Reynolds number conditions requires a miniature devices and finer measurements, which is complicated and costly, so the numerical simulation is an alternate approach to reduce the time and the cost. Many numerical studies optimizing control parameters, such as the jet location, the size and the jet velocity of the suction/blowing, were conducted researchers [12-15]. Sedar and Kaynak [16] investigated the blowing/suction control effects on NACA2415 airfoil at low Reynolds number conditions for a fixed angle of attack. Results indicated that smaller velocity is better for the blowing case; whereas larger velocity is better for the suction case. The performance of the airfoils can be considerably improved by combining the suction and the blowing control. Brehm et al. [17], show that the simultaneous use of suction and blowing is more effective than using the suction and the blowing separately. Huang et al. [18], studied numerically the suction and the blowing control on NACA0012 airfoil at an angle of attack of 18° and they concluded that suction is different from blowing. While the suction increases the lift by creating a larger and lower pressure zone on the airfoil, leading edge blowing increases lift by generating greater circulation about the separation bubble.

In the present contribution, a CFD solver based on a finite volume formulation, was developed to solve the full Navier-stokes equations in orthogonal curvilinear form. The numerical study is conducted for a flow over a NACA0012 airfoil operating at a low Reynolds number. Velocity profiles, skin friction distribution and flow pattern, for different angles of attack, are plotted in order to determine the position and the size of the separated region. The aerodynamic coefficients are then evaluated to examine the separation effect on the airfoil performance. The control of the separation is investigated using a parabolic distribution blowing along the separated region. The benefits of the control process is viewed through the flow structure and the aerodynamic performances compared with the uncontrolled case.

2. NUMERICAL METHOD

2.1. Governing equations

The flow is assumed two-dimensional, unsteady, incompressible and viscous. Since the Reynolds number investigated is very low, a fully laminar flow along the airfoil is considered. The governing equations are transformed into an orthogonal curvilinear coordinate system (ξ,η), such that the coordinates are aligned to the airfoil surface. The following are the non-dimensional equations expressing the mass and momentum conservation [19]:

Continuity equation

$$\frac{1}{h_1 h_2}\frac{\partial}{\partial \xi}\left(h_2 V_\xi\right)+\frac{1}{h_1 h_2}\frac{\partial}{\partial \eta}\left(h_1 V_\eta\right)=0 \tag{1}$$

Momentum equation in ξ direction

$$\begin{aligned}
&\frac{\partial V_\varepsilon}{\partial t}+\frac{1}{h_1 h_2}\frac{\partial}{\partial \varepsilon}\left(h_2 V_\varepsilon V_\varepsilon\right)+\frac{1}{h_1 h_2}\frac{\partial}{\partial \eta}\left(h_1 V_\varepsilon V_\eta\right)= \\
&-\frac{1}{h_1}\frac{\partial p}{\partial \varepsilon}+\frac{1}{Re\, h_2^2}\frac{\partial}{\partial \eta}\left(\frac{V_\varepsilon}{h_1}\right)\frac{\partial h_1}{\partial \eta}-\frac{2}{Re\, h_1 h_2^2}\frac{\partial V_\eta}{\partial \eta}\frac{\partial h_2}{\partial \varepsilon} \\
&+\frac{2}{Re\, h_1 h_2}\frac{\partial}{\partial \varepsilon}\left(\frac{h_2}{h_1}\frac{\partial V_\varepsilon}{\partial \varepsilon}\right)+\frac{1}{Re\, h_1 h_2}\frac{\partial}{\partial \eta}\left(\frac{h_1}{h_2}\frac{\partial V_\varepsilon}{\partial \eta}\right) \\
&+\frac{2}{Re\, h_1 h_2}\frac{\partial}{\partial \varepsilon}\left(\frac{V_\eta}{h_1}\frac{\partial h_1}{\partial \eta}\right)+\frac{1}{Re\, h_1 h_2}\frac{\partial}{\partial \eta}\left[h_2\frac{\partial}{\partial \varepsilon}\left(\frac{V_\eta}{h_2}\right)\right] \\
&-\frac{1}{Re\, h_1 h_2}\frac{\partial}{\partial \eta}\left(\frac{V_\varepsilon}{h_2}\frac{\partial h_1}{\partial \eta}\right)+\frac{1}{Re\, h_1^2}\frac{\partial}{\partial \varepsilon}\left(\frac{V_\eta}{h_2}\right)\frac{\partial h_1}{\partial \eta} \\
&-\frac{V_\varepsilon V_\eta}{h_1 h_2}\frac{\partial h_1}{\partial \eta}+\frac{V_\eta^2}{h_1 h_2}\frac{\partial h_2}{\partial \varepsilon}-\frac{2V_\varepsilon}{Re\, h_1^2 h_2^2}\left(\frac{\partial h_2}{\partial \varepsilon}\right)^2
\end{aligned} \tag{2}$$

Momentum equation in η direction

$$\frac{\partial V_\eta}{\partial t}+\frac{1}{h_1h_2}\frac{\partial}{\partial \varepsilon}\left(h_2 V_\varepsilon V_\eta\right)+\frac{1}{h_1h_2}\frac{\partial}{\partial \eta}\left(h_1 V_\eta V_\eta\right)=$$
$$-\frac{1}{h_2}\frac{\partial p}{\partial \eta}+\frac{1}{Re\,h_1^2}\frac{\partial}{\partial \varepsilon}\left(\frac{V_\eta}{h_2}\right)\frac{\partial h_2}{\partial \varepsilon}-\frac{2}{Re\,h_1^2h_2}\frac{\partial V_\varepsilon}{\partial \varepsilon}\frac{\partial h_1}{\partial \eta}$$
$$+\frac{1}{Re\,h_1h_2}\frac{\partial}{\partial \varepsilon}\left(\frac{h_2}{h_1}\frac{\partial V_\eta}{\partial \varepsilon}\right)+\frac{2}{Re\,h_1h_2}\frac{\partial}{\partial \eta}\left(\frac{h_1}{h_2}\frac{\partial V_\eta}{\partial \eta}\right)$$
$$+\frac{1}{Re\,h_1h_2}\frac{\partial}{\partial \varepsilon}\left[h_1\frac{\partial}{\partial \eta}\left(\frac{V_\varepsilon}{h_1}\right)\right]+\frac{2}{Re\,h_1h_2}\frac{\partial}{\partial \eta}\left(\frac{V_\varepsilon}{h_2}\frac{\partial h_2}{\partial \varepsilon}\right)$$
$$-\frac{1}{Re\,h_1h_2}\frac{\partial}{\partial \varepsilon}\left(\frac{V_\eta}{h_1}\frac{\partial h_2}{\partial \varepsilon}\right)+\frac{1}{Re\,h_2^2}\frac{\partial}{\partial \eta}\left(\frac{V_\varepsilon}{h_1}\right)\left(\frac{\partial h_2}{\partial \varepsilon}\right)$$
$$-\frac{V_\varepsilon V_\eta}{h_1h_2}\frac{\partial h_2}{\partial \varepsilon}+\frac{V_\varepsilon^2}{h_1h_2}\frac{\partial h_1}{\partial \eta}-\frac{2V_\eta}{Re\,h_1^2h_2^2}\left(\frac{\partial h_1}{\partial \eta}\right)^2 \qquad (3)$$

here h_1 and h_2 are the metric stretching factors:

$$h_1=\sqrt{\left(\frac{\partial x}{\partial \xi}\right)^2+\left(\frac{\partial y}{\partial \xi}\right)^2}\ ,h_2=\sqrt{\left(\frac{\partial x}{\partial \eta}\right)^2+\left(\frac{\partial y}{\partial \eta}\right)^2}$$

The physical velocities are related to the computational velocities by the following relations:

$$U=\frac{1}{h_1}\left(\frac{\partial x}{\partial \xi}\right)V_\xi+\frac{1}{h_2}\left(\frac{\partial x}{\partial \eta}\right)V_\eta$$
$$V=\frac{1}{h_1}\left(\frac{\partial y}{\partial \xi}\right)V_\xi+\frac{1}{h_2}\left(\frac{\partial y}{\partial \eta}\right)V_\eta$$

The no-slip and no-penetration boundary conditions are applied on the airfoil surface for the clean case (without control) . The blowing control is prescribed through wall-normal velocity on the surface of the airfoil at the separated region. The far-field boundary condition is applied at the outlet of the computational domain, so that the velocity at the boundary is equal to U_0.

2.2. Grid generation

Orthogonal conformal grid generation with an O-type topology is obtained by applying the Von Karman-Trefftz transformation [20]. Various grid resolutions are tested to ensure the grid independence of the flow solution. The total number of 33,000 cells is adopted, since the solution exhibits negligible change with farther increase in the number of nodes. The far-field boundary is located at a distance 20 times the chord length, away from the airfoil surface. The grids are clustered near the airfoil surface in the wall-normal direction to resolve the steep gradients within the boundary layer and to capture the physical phenomenon more accurately (Figure. 1).

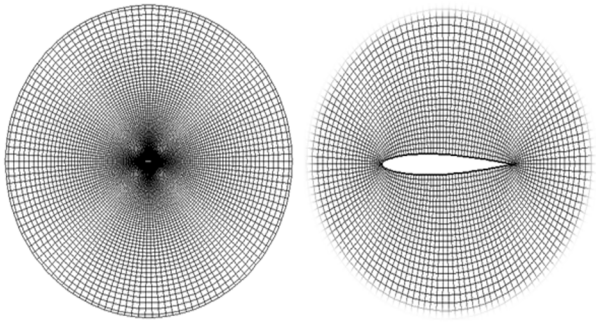

Figure 1. Structured grid around the airfoil

2.3. Numerical schemes

The discretization of the governing partial differential equations is based on the finite volume structured formulation [21-22]. The major advantage of the finite volume method is that the conservation laws are verified both locally on each finite volume and globally on the whole computational domain. The computational domain is decomposed into quadrilateral elements, the pressure is stored at the nodes and the two components of the velocity vector are stored at the cell faces in between the nodes. This way, the obtained staggered grid storage of the dependent variables, avoid the pressure field oscillations. A second-order accurate Adam-Bashforth scheme is applied for the time integration and a second-order accurate central difference scheme is applied for the convective terms discretization. The SIMPLER algorithm coupled with a staggered storage of the dependent variables, is used in order to handle the lake of a proper pressure equation. The resulting algebraic equations system is solved using the cyclic Thomas algorithm [23].

3. RESULTS

The code program implemented in fortran-90 language, includes six modules and performs calculations in double precision format. The program is developed to solve the 2-D, time dependent, laminar and incompressible Navier-Stokes equations in orthogonal curvilinear coordinates and can be applied to bodies of complex geometry shapes, to compute the flow characteristics and the aerodynamic coefficients.

3.1. Code validation

The solver is tested for the case of a flow about a circular cylinder to predict the boundary layer separation for a Reynolds number Re=1000. At a dimensionless time τ corresponding to 500 000 time steps, two separation cells appear at the back of the cylinder (Fig. 2).

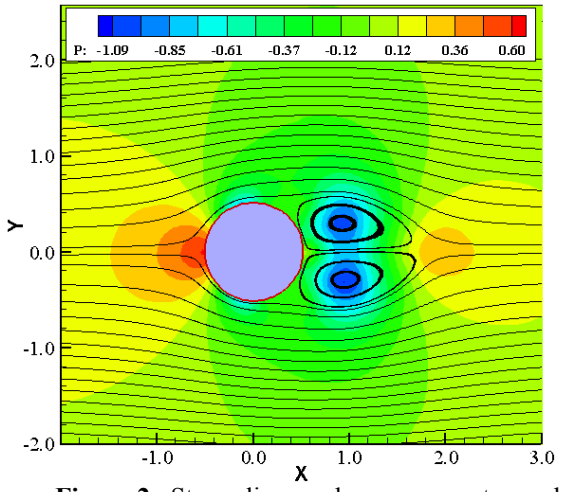

Figure 2. Streamlines and pressure contours about a circular cylinder for Re=1000

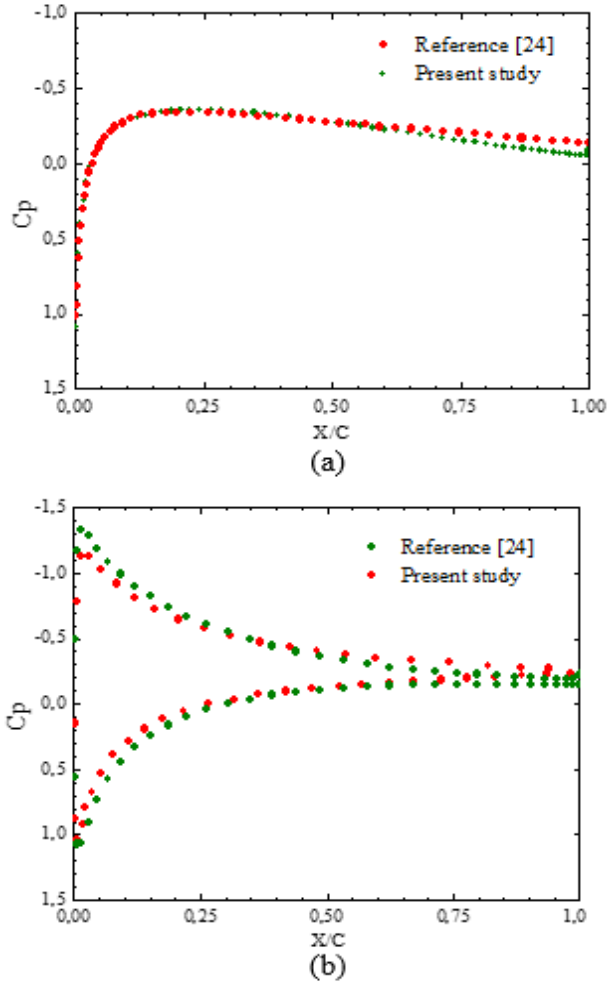

Figure 3. Cp distribution over NACA0012 for Re=500: (a) α=0°, (b) α=10°

A second validation of the solver is performed by applying it to compute the pressure coefficient distribution along a NACA0012 airfoil at a Reynolds number of 500, for two different angles of attack of 0° and 10°. The present simulations are compared with those obtained by Hafez et al. [24], for the same Reynolds number and the same angles of attack. Figure 3 illustrates the good agreement between the obtained results and those of the referenced study. It is worth noting that the maximum discrepancy is less than 5%, despite the different mathematical models used in the two studies. In the present study, the full Navier-Stokes equations are solved in the whole computational domain, while in the referenced study, the domain is divided to a viscous layer and an external potential layer.

The drag coefficient Cd predicted at a Reynolds number of 500 and an angle of attack of 0°, reported by Lockard et al. [25] is 0.1758 and the one predicted by Peng et al. [26] is 0.1760. These two results are in good agreement with the Cd obtained by the present study (Cd=0.1750).

3.2. Boundary layer separation

The main attention in this part of the study is paid to the location of the boundary layer separation point, the size and the strength of the separation bubble. The separation point is defined as the location where the wall shear stress is equal to zero with the apparition of an inflexion point on the velocity curve. The strength of the separation is defined as the ratio of the maximum reversed flow velocity to the mean flow velocity. The possibility of the reattachment of the separated layer is related to the amount of the momentum transferred to the separated region. If the amount of this momentum is sufficient to cause the necessary pressure rise to overcome the adverse pressure gradient, the reattachment will occur. At a relatively low Reynolds number, the transferred momentum may be insufficient to overcome the adverse pressure gradient and the separated layer may remain detached. These parameters of the separation are studied through the velocity profiles, the skin friction distribution and the streamlines distribution. First, velocity profiles as a function of the dimensionless wall-normal coordinates were computed in the boundary layer at three chordwise locations on the airfoil; x/c=0.6, 0.8 and 0.95 for the angles of attack between 0° and 15°. In Figure 4 the angle of attack is 8°, the velocity profile curve shows only an inflexion at x/c=0.95 chord length from the leading edge, indicating the separation point of the boundary layer. At 12°, as shown in Figure. 5, the strength of the separation is about 5% at x/c=0.8 and 10% at x/c=0.95. At 15°, shown in Figure 6, the strength of the separation is 5% at x/c=0.6, 10% at x/c=0.8 and almost 20% at x/c=0.95.

The location of the boundary layer separation can be also viewed from the distribution of the skin friction coefficient along the airfoil surface, for different angles of attack. The location of the separation point is defined by a zero skin friction coefficient. Figure 7 shows the skin friction distribution for different angles of attack. It can be seen from this latter figure that for 0° and 5° the skin friction is different from zero, showing that the separation does not occur. However, the skin friction on the suction side of the airfoil vanishes from x/c=0.85 at 8° of the angle of attack, x/c=0.65 at 10°, x/c=0.5 at 12° and x/c=0.3 at 15°, indicating that the separation point advances towards the leading edge as the angle of attack is raised.

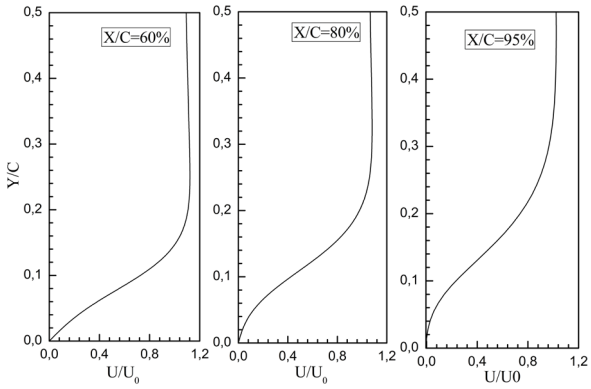

Figure 4. Velocity profiles at α=8°

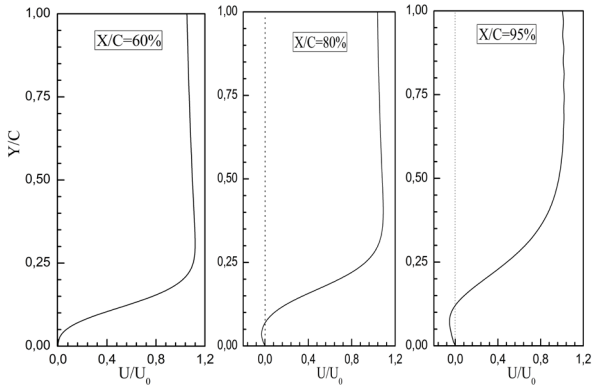

Figure 5. Velocity profiles at α=12°

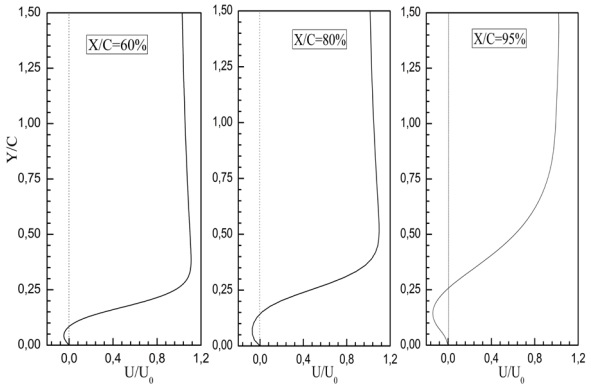

Figure 6. Velocity profiles at α=15°

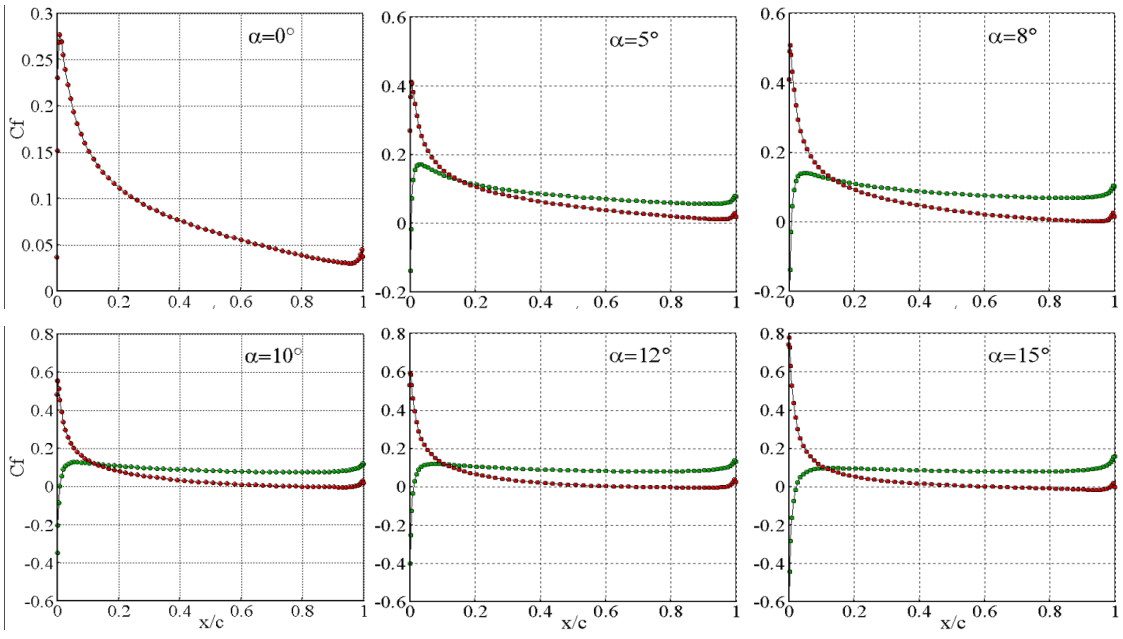

Figure 7. Skin friction coefficient distribution over a NACA0012 airfoil at Re=500, suction side (red), pressure side (green)

Streamlines distribution at different angles of attack gives a clear view of the minimum onset angle leading to separation and the evolution of the separated zone as the angle of attack is increasing (Fig. 8). At 8°, a small separation bubble appears near the trailing-edge of the airfoil. A further increase in the angle of attack causes an increase in the size of the separation bubble and the separation point moves towards the leading-edge. The location of the separation point for different angles of attack shown on the flow pattern is almost the same location predicted by the velocity profiles and the skin friction distribution.

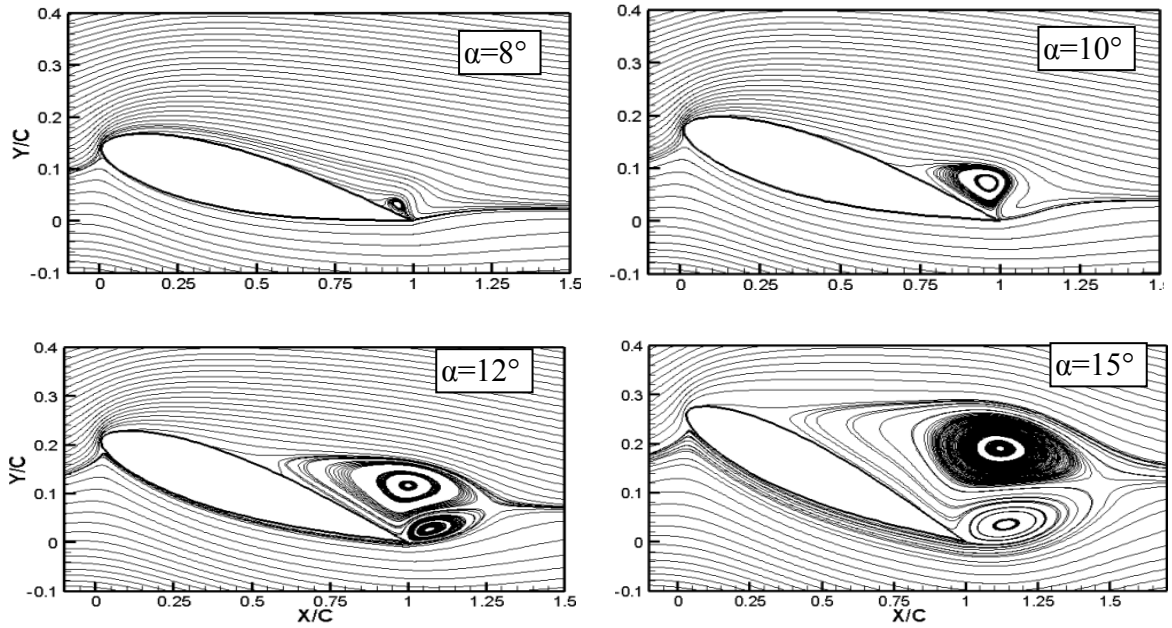

Figure 8. Streamlines representation about a NACA0012 airfoil at Re=500

3.3. Boundary layer separation control

The separated region investigated above is controlled using a parabolic distribution blowing. A tangential blowing is performed along the separated region. The blowing angle and position are chosen according to an earlier research published by Huang et al. [27]. The authors studied separately the suction and the blowing on a NACA0012 airfoil and concluded that the delay of the separation is more effective when a perpendicular suction is applied near the leading edge or a tangential blowing applied on the suction side of the airfoil. In the actual study, a parabolic distribution of the jet velocity ratio was opted in order to avoid the abrupt gradients velocity between the clean and the controlled surfaces. The graph illustrated in Figure 9a, shows the lift variations with the angle of attack without (baseline) and with blowing control for jet velocity ratio ranging from 0.1 to 0.3. The effect of the separation on the lift coefficient is presented by the baseline curve where the lift coefficient keeps increasing almost linearly up to the angle of attack of 8°. However, beyond α equal to 8°, a significant decrease in the slope of the lift curve can be seen, indicating the start of the boundary layer separation. The drop of the lift slope given by dCl/dα, has been estimated to be about 23%.

As the control is applied, a significant increase in the lift coefficient can be clearly seen. At an angle of attack α=12° and for a maximum blowing velocity ratio ϕ=0.3, a 22% increase in the lift coefficient is obtained.

The baseline curve shown in Figure 9b illustrates the loss in the lift to drag ratio, caused by the separation. The coefficient Cl/Cd increases rapidly before separation and slows down suddenly just beyond the onset separation angle α= 8°. The increase of the jet blowing velocity improves the maximum lift coefficient and affects moderately the drag coefficient, so the overall performances are improved with an increase of 7.55% in the lift to drag ratio reached for ϕ equal to 0.3 (Table 1). It was noticed that the higher the angles of attack, the more is the improvement of Cl/Cd.

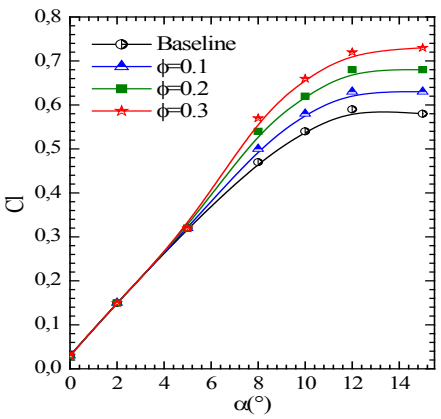

(a)

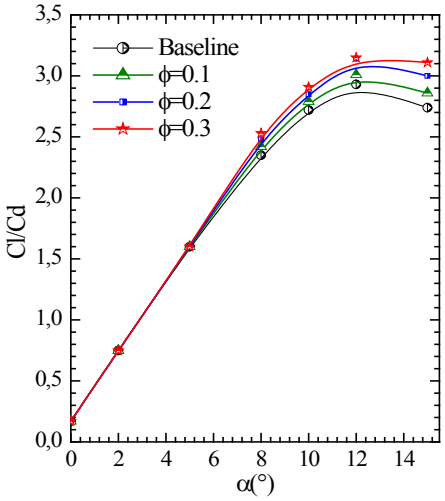

(b)

Figure 9. Effect of blowing control on NACA0012 aerodynamic performances

ϕ	*Cl*	*Cd*	*Cl/Cd*	*%Cl*	*%Cl/Cd*
0,0	0,59	0.20	2,93	---	---
0,1	0,63	0.21	3,01	7,58	2,78
0,2	0,68	0.22	3,14	15,50	7,19
0,3	0,72	0.23	3,15	21,87	7,55

Table 1: Dependence of the aerodynamic coefficients on velocity control at α=12°

The reverse flow obtained for different angles of attack at a location x/c=0.95 (Fig. 10), indicates that the effectiveness of the blowing control depends on the angle of attack and blowing velocity ratio. The higher the angle of attack the bigger the jet blowing ratio should be applied to eliminate the reverse flow. As it can be seen for α=15°, even for ϕ=0.3, the reverse flow is still present.

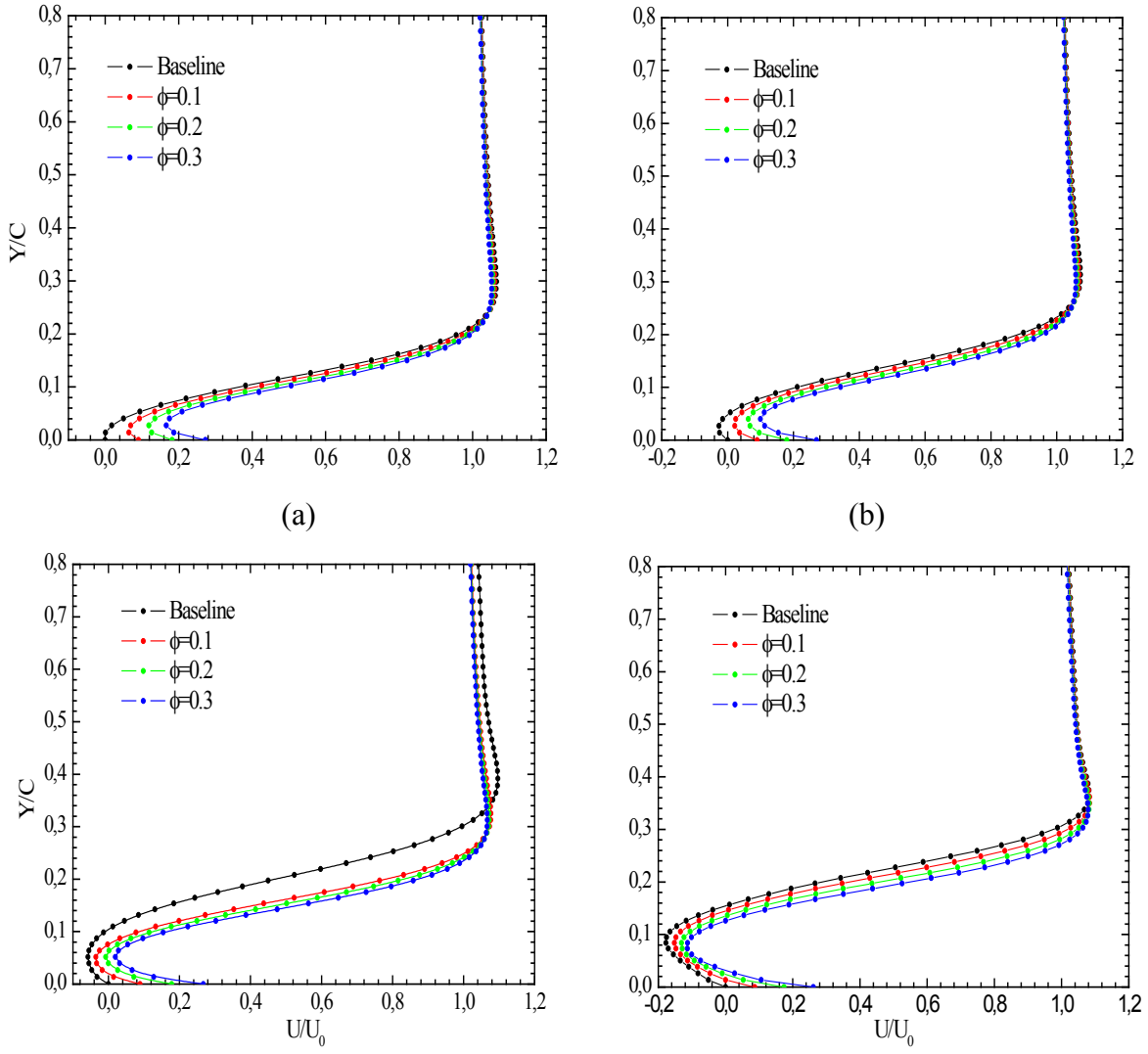

(a) (b) (c) (d)

Figure 10. Effect of blowing control on velocity profiles at different angles of attack: (a) α=8°, (b) α=10°, (c) α=12°, (d) α=15°

The control effect of the maximum velocity ratio on the flow structure for an angle of attack of 12°, is shown in figure 11. When the control process is applied with a blowing velocity ratio ϕ=0.1, the separation point initially located at 0.6 chord length from the leading edge, moves to 0.75 location with a significant reduction of the separation bubble size. As ϕ is increased to 0.2, the separation point goes more downward towards the trailing edge reaching the 0.85 chord length location. With a further increase of the blowing velocity up to 0.3 the separation bubble is completely suppressed.

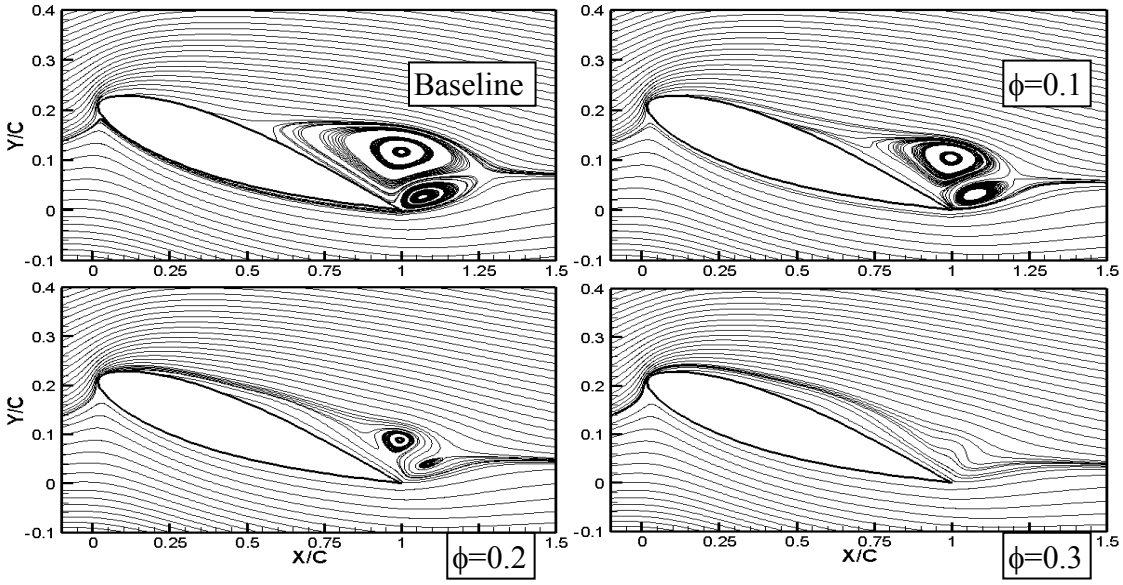

Figure 11. control velocity ratio effect on the separated region for an angle of attack α=12°

4. CONCLUSION

A numerical simulation has been carried out to study the separation of the boundary layer on a NACA0012 airfoil for a very low Reynolds number of 500. The computations were performed for different angles of attack. The finite volume method was used to discretize the incompressible full Navier-Stokes equations, written in curvilinear coordinates. For this purpose, a computer program has been developed. To handle the complexity of the airfoil geometry, a procedure for the orthogonal grid generation based on the conformal mapping, is combined to the solver. The accuracy of the developed solver has been tested for the case of the flow about a circular cylinder and in computing the pressure coefficient distribution along a NACA0012 airfoil. The solver makes it possible to predict the boundary layer separation through the velocity profiles, the skin friction distribution and the flow structure. It has been found that the separation zone begins to appear at an angle of attack of 8°. As the angle of attack increases the separated zone grows up and moves towards the leading-edge of the airfoil. It should be noted that the flow separation affects substantially the aerodynamic performances. The lift coefficient slope is reduced by about 23% and the lift to drag ratio slope is reduced by about 26%, just beyond the angle of attack at which the separation begins. The application of the boundary layer control concept using different tangential blowing velocities along the separation region, has demonstrated its effectiveness by delaying the separation bubble towards the trailing edge till its complete elimination for a blowing velocity ratio ϕ equal to 0.3. Thus, the overall aerodynamic performances have been improved by 22% in the maximum lift coefficient and by 7.5% in the lift to drag ratio.

REFERENCES

[1] S. Yarusevych, .J. G. Kawall, P. E. Sullivan, Separated-Shear-Layer development on an airfoil at low Reynolds numbers, AIAA Journal, 46 (2008) 3060-3069.

[2] W. Shyy et al, Computational aerodynamics of low Reynolds number plunging pitching and Flexible Wings for MAV Applications, 46th AIAA Aerospace science meeting and exhibit, January 7-10, 2008, Reo, NEVADA.

[3] Md. Mahbub, Y. Zhou, H. V. Yang, The ultra-low Reynolds number airfoil wake, Experimental Fluids, 48 (2010) 81-103.

[4] P. L. Delafin, F. Deniset, J. A. Asotolfi, Effect of the laminar separation bubble induced transition on the hydrodynamic performance of a hydrofoil, European Journal of mechanics B/Fluids, 46 (2014) 190-200.

[5] H. Shan, L Jiang, C. Liu, Direct numerical simulation of flow separation around a NACA0012 airfoil, Computers & Fluids, 34 (2005) 1096-1114.

[6] M. Alam, ND. Sandham, Direct numerical simulation of short laminar separation bubbles with turbulent reattachment, J. Fluid Mech, 410 (2000) 1-28.

[7] S. B. Hazra, A. Jamson, Aerodynamic shape optimization of airfoils in ultra-low Reynolds number flow using simultaneous pseudo-time stepping, Aerospace Computing Lab (ACL) report, 2007-4, 2007.

[8] W. Yuan, M. Khalid, J. Windte, U. Scholz, R. Radespiel, Computational and experimental investigations of low-Reynolds-number flows past an airfoil, The Aeronautical Journal, 111 (2007) 17-29.

[9] Y. Zhou, M. M. Alam, H. X. Yang, H. Guo, D. H. Wood, International Journal of Heat and fluid flow, 32 (2011) 329-339.

[10] S. Rajakumar, D. Ravindran, Computational fluid dynamics of wind turbine blade at various angles of attack and low Reynolds number, International Journal of Engineering Science and Technology, 2 (2010) 6474-6484.

[11] H. Shan, L. Jiang, C. Liu, M. Love, B. Maines, Numerical study of passive and active flow separation control over a NACA0012 airfoil, Computers & Fluids, 37 (2008) 975-992.

[12] K. Yousefi, S. R. Saleh, P. Zahedi, Numerical Study of flow separation control by tangential and perpendicular blowing on the NACA0012 airfoil, International Journal of Engineering, 7 (2013) 10-24.

[13] R. Wahidi, and D. Briges, Effects of distributed suction on an airfoil at low Reynolds number, AIAA Journal, 50 (2012) 523-539.

[14] Y. Hoarau, M. Braza, Y. Ventikos, D. Faghani, First stages of the transition to turbulence and control in the incompressible detached flow around a NACA0012 wing, International Journal of Heat and Fluid Flow, 27 (2006) 878-886.

[15] R. Azima, M. Hasana, M. Alib, Numerical investigation on the delay of boundary layer separation by suction for NACA 4412, Procedia Engineering, 105 (2015) 329-334.

[16] M. Serdar Genç, C. Kaynak, Control of laminar separation bubble over NACA2415 aerofoil at low Re transitional flow using blowing/suction, 13th International Conference on Aerospace Sciences & Aviation Technology, May 26-28, 2009, Cairo, Egypt.

[17] C. Brehm, A. Gross, H. F. Fasel, Open loop flow-control investigation for airfoils at low Reynolds numbers, AIAA Journal, 51 (2013) 1843-1860.

[18] L. Huang, P. G. Huang, R. P. LeBeau, Numerical study of blowing and suction control mechanism on NACA0012 airfoil, Journal of Aircraft, 41 (2004) 1005-1013.

[19] D. A. Anderson, J. C. Tannehill, R. H Pletcher, Computational Fluid Mechanics and Heat Transfer, Hemisphere Publishing Corporation, 1984.

[20] V. Kitsios, D. Rodriguez, V. Theofilis, A. Ooi, J. Soria, Journal of Computational Physics, 228 (2009) 7181-7196.

[21] S. V Patankar, Numerical heat transfer and fluid flow, Hemisphere Publishing Corporation, New York, 1980.

[22] S. Koshizuka, Y. Oka, S. Kondo, A staggered differencing technique on boundary curvilinear grids for incompressible flows along curvilinear or slant walls, Journal of Computational Mechanics, 7 (1990) 123-136.

[23] H. K. Versteeg, W. Malalasekera, An introduction to computational fluid dynamics: The finite volume method, Longman Group Ltd, Harlow, England, 1995.

[24] M. Hafez, A. Shatalov, E. Wahba, Numerical simulations of incompressible aerodynamic flows using viscous/inviscid interaction procedures, Comput. Methods Appl. Mech. Engrg., 195 (2006) 3110-3127.

[25] D. P. Lockard et al., Evaluation of PowerFlow for aerodynamic applications, Journal of statistical physics, 107 (2002) 423-478.

[26] Y. Peng et al., Application of multi-block approach in the immersed boundary-lattice Boltzmann method for viscous fluid flows, Journal of computational physics, 218 (2006) 460-478.

[27] L. Huang, R. P. LeBeau, P. G. Huang, Optimization of blowing and suction control on NACA 0012 airfoil using genetic algorithm, 42nd AIAA Aerospace Sciences Meeting and Exhibit, January 5-8, 2004, Reno, Nevada.